Soft Chemical Fabrication and Material Characterization of Mn Doped SnO$_2$ Ceramic Nanostructures for Application in Photocatalysis

Niviya Rajan[a], Arputharaj Samson Nesaraj[a,b]* & Manasai Arunkumar[a]

[a]Department of Chemistry, Karunya Institute of Technology and Sciences (Deemed to be University), Karunya Nagar, Coimbatore, Tamil Nadu– 641 114, India
[b]Department of Chemistry, School of Advanced Sciences, Kalasalingam Academy of Research and Education (Deemed to be University), Anand Nagar, Krishnankoil, Tamil Nadu- 626 126, India

In this research work, a simple soft chemical synthesis route is adopted to synthesize (Sn$_{1-x}$Mn$_x$O$_{2-\delta}$; where x=0, 0.05, 0.10, 0.15 and 0.20) based ceramic nanoparticles. The prepared nanoparticles were characterized to X-ray diffraction (XRD), FTIR spectroscopy, particle size analysis, SEM, EDAX, UV and photoluminescence (PL) studies. From XRD, the crystalline geometry of ceramic nanoparticles was found to be tetragonal. FTIR data have shown a broad absorption band at a wavelength of ~ 600 cm^{-1} due to M-O stretching vibration mode. The ceramic nanoparticles were found to be in the range of 704 to 1258 nm. Smaller grains (<100 nm) along-with few bulky grains were reported by SEM. The absorption of ceramic particles was found maximum at 283 nm as per UV spectra. PL spectra exhibited a strong peak at 432 nm. The photocatalysis was studied to degrade methylene blue dye present in water sample using the ceramic nanoparticles under UV, visible and sun lights. Among the samples studied, Sn$_{0.95}$Mn$_{0.05}$O$_{2-\delta}$ exhibited better photocatalytic degradation behavior (84.8%) under visible light after 120 minutes of irradiation.

Keywords: Mn doped SnO$_2$; Chemical Synthesis; Characterization; Photocatalysis; Methylene Blue

1 Introduction

Nanoceramic metal oxide particles have gained interest now-a-days because of their tuning physico-chemical properties. Their material characteristics are highly dependent on various parameters, such as, functional, spectral and particle and microstructural phenomena[1]. It was reported that if the particle size decreases, the band structure of the ceramic materials may also undergo changes[2]. It was found that the nanopartilces can behave differently especially from their bulk[3]. Ceramic metal oxides can find application in many advanced fields, such as catalytic[4], magnetic[5], electrochemical sensor[6], coatings[7], biomedical[8], biological imaging[9], agriculture[10] and so on. Apart from the above applications, nanoceramic oxides can be adopted effectively for treating water and wastewater by using adsorption phenomena[11]. Nanoceramic semiconductor metal oxides have been proposed for other technological applications also because of their shape and particulate dependent physico-chemical properties[12]. Among them, SnO$_2$ nanoceramic particles have become the highly efficient one, since its extensive applications in multiple hi-tech areas[13]. It was reported recently that the scientific applications of tin oxide nanoceramic particles mainly based on their structural, morphological and particulate characteristics[14].

Different techniques have been reported to prepare tin oxide nanostructures, viz., sol-gel[15], chemical digestion[16], precipitation[17], microwave heating[18], hydrothermal[19], autoclave[20], and so on. Tin oxide has been prepared in different morphological structures, such as, nanosheets[21], nanotubes[22], nanorods[23], nanowires[24], nanoflowers[25], nanofibers[26] and so on. In this research paper, we report the simple methodology of synthesis and characterization of Mn doped SnO$_2$ nanostructures (Sn$_{1-x}$Mn$_x$O$_{2-\delta}$; where x=0, 0.05, 0.10, 0.15 and 0.20) as a first part. In the second part, we report their application as photocatalysts in the removal of toxic methylene blue dye present in the water sample. The obtained results were presented and discussed in this research article.

2 Materials and Methods

2.1 Chemicals Used

The analytical grade chemicals such as tin chloride (SnCl$_2$) (97% Merck, India), manganese (II) nitrate tetrahydrate (Mn(NO$_3$)$_2$.4H$_2$O) (99%, Merck, India),

sodium hydroxide (97%,Merck, India), sodium dodecyl sulfate (SDS)(98%, Merck, India) and ethyl alcohol (99.9%, Changshu Yangyuan, China).

2.2 Soft Chemical Synthesis

The Mn doped SnO_2 nanoparticles were prepared by soft chemical method. In the beginning, appropriate concentration of NaOH in 100 mL was prepared. To this solution, 3 ml of 3% SDS surfactant solution was added in order to control the particulate properties of the ceramic materials. To this solution mixture the appropriate strength of tin chloride solution along-with manganese nitrate solution was added slowly with continuous stirring for about two hours in a magnetic stirrer set-up. The entire reagent mixing was completed at ~28 ^{o}C. During the addition of aqueous salt solution, the pH may reach the acidic pH level which may result in poor precipitation reaction. To avoid this, the pH of the entire solution was kept above 9 by the addition of alkali. The resultant precipitate mixture ($Sn(OH)_2$ + $Mn(OH)_2$) was filtered and washed with pure water: ethanol mixture (9:1 v/v) for about 5 – 10 times. The washed product was dried at 60 ^{o}C in air oven for whole night. Then, the dried product was calcined in a furnace at different temperatures, viz., 150, 300, 450 and 600 ^{o}C for 2 hours each. During the high temperature calcination, unwanted organic impurities were completely removed and ultra-pure Mn doped SnO_2 nanoparticles were resulted. The flow chart to fabricate the materials by soft chemical method is presented in Fig. 1. The list of reagents used in this process is given in Table 1. The chemical reaction involved in the preparation of Mn doped SnO_2 nanoparticles is given in Equation 1.

$$2NaOH_{(aq)} + (1-x)\ SnCl_{2(aq)} + x\ Mn(NO_3)_{2(aq)} \rightarrow Sn_{1-x}Mn_xO_{2-\delta\ (s)} + (2-2x)\ NaCl_{(aq)} + 2x\ NaNO_{3(aq)} + yH_2O_{(g)} \uparrow$$
$$...(1)$$
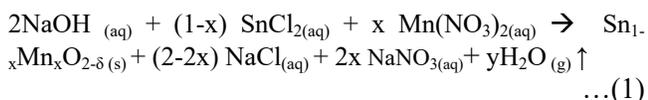
(where x = 0, 0.1, 0.2, 0.3 and 0.4)

2.3 Characterization

The powder XRD studies were done with a Shimadzu XRD6000 X-ray diffractometer. The crystallite sizes of manganese doped tin oxide were found out using the Debye-Scherrer equation. The FTIR spectra were recorded by Shimadzu FTIR Spectrophotometer using KBr pellet technique. The average particle size was measured with a Zetasizer Ver. 6.32. The surface characteristics were studied by SEM JEOL JSM-6610. The UV curves were recorded by UV-Visible Double Beam Spectrophotometer Shimadzu 1800. Powder samples were taken in a quartz cell and spectra were recorded in the range between 200 nm to 600 nm by using diffused reflectance method. Photoluminescence spectra were taken by Spectroflurophotometer (Horiba Jobin Yvon, Fluorolog-3) with Xe laser as the excitation light source at room temperature.

3 Results and Discussion

3.1 XRD Studies

The powder XRD patterns obtained on manganese doped SnO_2 nanoparticles are indicated in Fig. 2. The
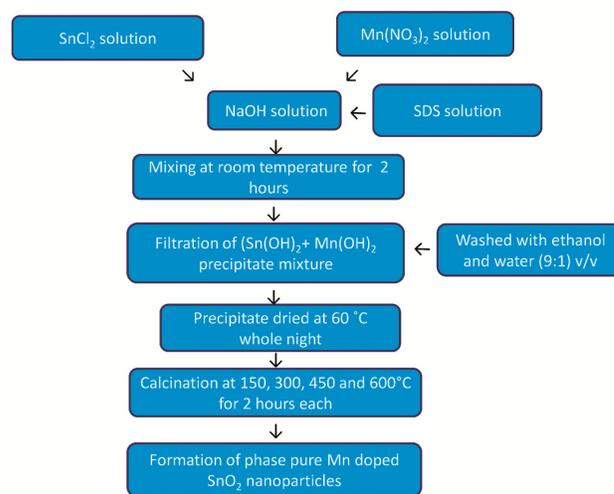
Fig. 1 — Flow chart to prepare Mn doped SnO_2 nanoparticles.

Precursor materials / SnO_2 based materials	SnO_2	$Sn_{0.95}Mn_{0.05}O_{2-\delta}$	$Sn_{0.90}Mn_{0.10}O_{2-\delta}$	$Sn_{0.85}Mn_{0.15}O_{2-\delta}$	$Sn_{0.80}Mn_{0.20}O_{2-\delta}$
Concentration of $SnCl_2$ Solution/ Wt.(g)	0.10 M / 2.25 g	0.095 M / 2.143 g	0.090 M / 2.03112 g	0.085 M / 1.9182 g	0.080 M / 1.8054 g
Concentration of $Mn(NO_3)_2$/ Wt. (g)c	---	0.005 M / 0.125 g	0.010 M / 0.251 g	0.015 M / 0.3765 g	0.020 M / 0.5020 g
Concentration of NaOH / Wt. (g)	0.20M / 0.80 g	0.20M / 0.80 g	0.20 M / 0.80 g	0.20 M / 0.80 g	0.20 M / 0.80 g

Table 1 — Reagents used in this process

Table 2 — XRD data obtained on Mn doped SnO$_2$ nanoparticles

Sample	Crystal structure	Unit cell lattice parameters (Å)	Unit cell volume (Å)^3	Crystallite size (nm)
SnO$_2$	Tetragonal	a=4.72498 c =3.18739	71.1598	2.792
Sn$_{0.95}$Mn$_{0.05}$O$_{2-\delta}$	Tetragonal	a=4.73645 c=3.18132	71.1852	9.193
Sn$_{0.90}$Mn$_{0.10}$O$_{2-\delta}$	Tetragonal	a=4.73645 c=3.22790	72.4145	11.19
Sn$_{0.85}$Mn$_{0.15}$O$_{2-\delta}$	Tetragonal	a=4.75130 c=3.19170	72.0521	11.65
Sn$_{0.80}$Mn$_{0.20}$O$_{2-\delta}$	Tetragonal	a=4.71851 c=3.20209	71.2924	11.95
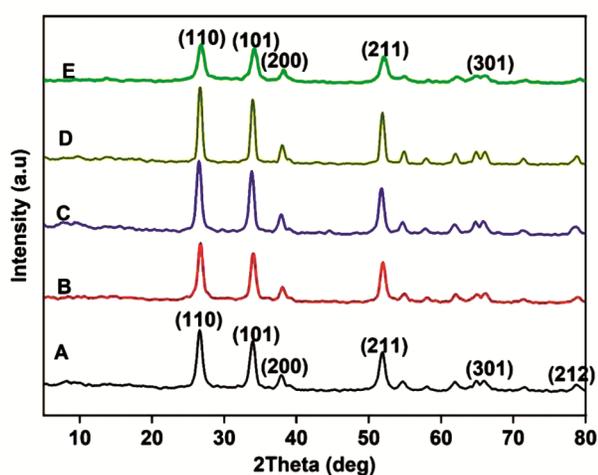
Fig. 2 — XRD patterns obtained on Mn doped SnO$_2$ nanoparticles (a) SnO$_2$; (b) Sn$_{0.95}$Mn$_{0.05}$O$_{2-\delta}$; (c) Sn$_{0.90}$Mn$_{0.10}$O$_{2-\delta}$; (d) Sn$_{0.85}$Mn$_{0.15}$O$_{2-\delta}$; (e) Sn$_{0.80}$Mn$_{0.20}$O$_{2-\delta}$.

Fig. 3 — FTIR spectra obtained on Mn doped SnO$_2$ nanoparticles (a) SnO$_2$; (b) Sn$_{0.95}$Mn$_{0.05}$O$_{2-\delta}$; (c) Sn$_{0.90}$Mn$_{0.10}$O$_{2-\delta}$; (d) Sn$_{0.85}$Mn$_{0.15}$O$_{2-\delta}$; (e) Sn$_{0.80}$Mn$_{0.20}$O$_{2-\delta}$.

XRD peaks of the ceramic particles were reported to be sharp which reflect the well crystalline behavior. The product was identified as SnO$_2$ using JCPDS pattern No.88-0287. The crystalline structure was confirmed as tetragonal phase of SnO$_2$. No impurity peaks were seen in the XRD patterns. It was reported that Sn$_{1-x}$Dy$_x$O$_2$ (x=0, 0.05 and 0.10) indexed in tetragonal crystal structure[27]. The XRD data obtained on the manganese doped tin oxide nanoparticles are given in the Table 2. The obtained parameters were in line with the reported literature[28].

3.2 FTIR Studies

The FTIR spectra obtained on Mn doped SnO$_2$ nanoparticles are shown in Fig. 3. From the FTIR spectra, it was understood that a peak appeared at around 600 cm^{-1} in all the samples which may be due to SnO$_2$ frame work. Similarly, the peaks appeared at 1640 and 3454 cm^{-1} may be due to the presence of moisture in the ceramic particles [29]. A peak appeared at around 1400 cm^{-1} may be attributed to C-H stretching and vibrations in the material because of few organic residues from C$_2$H$_5$OH or from surfactant[30].
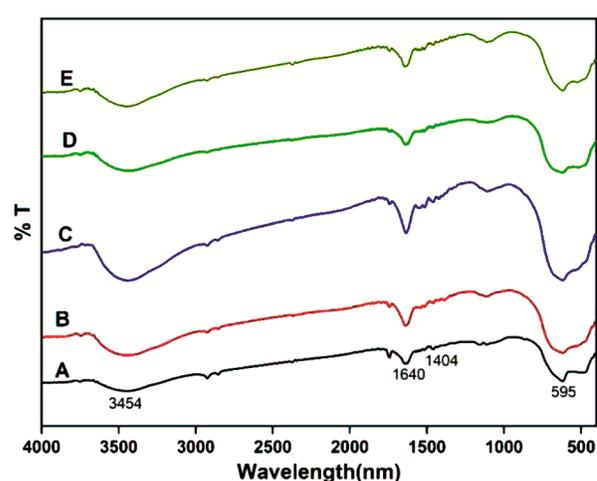
Particle characteristics

The particle size distribution curves obtained with manganese doped tin oxide nanoparticles are shown in Fig. 4. The particle characteristics data is indicated in Table 3. The data revealed the occurrence of nanosized grains along-with few micron sized grains (> 500 nm) in the samples. The size accumulation of particles can be controlled by choosing suitable surfactants with suitable concentration[31]. The surfactant used in this study (SDS) did not contribute much towards controlling the particle characteristics.

3.3 SEM Studies

The SEM images obtained with manganese doped tin oxide nanoparticles are shown in Figure 5. From the SEM photographs, the grain size was found to be in the range of 50 – 100 nm. However, agglomeration is seen in few places of the structures. Few micron
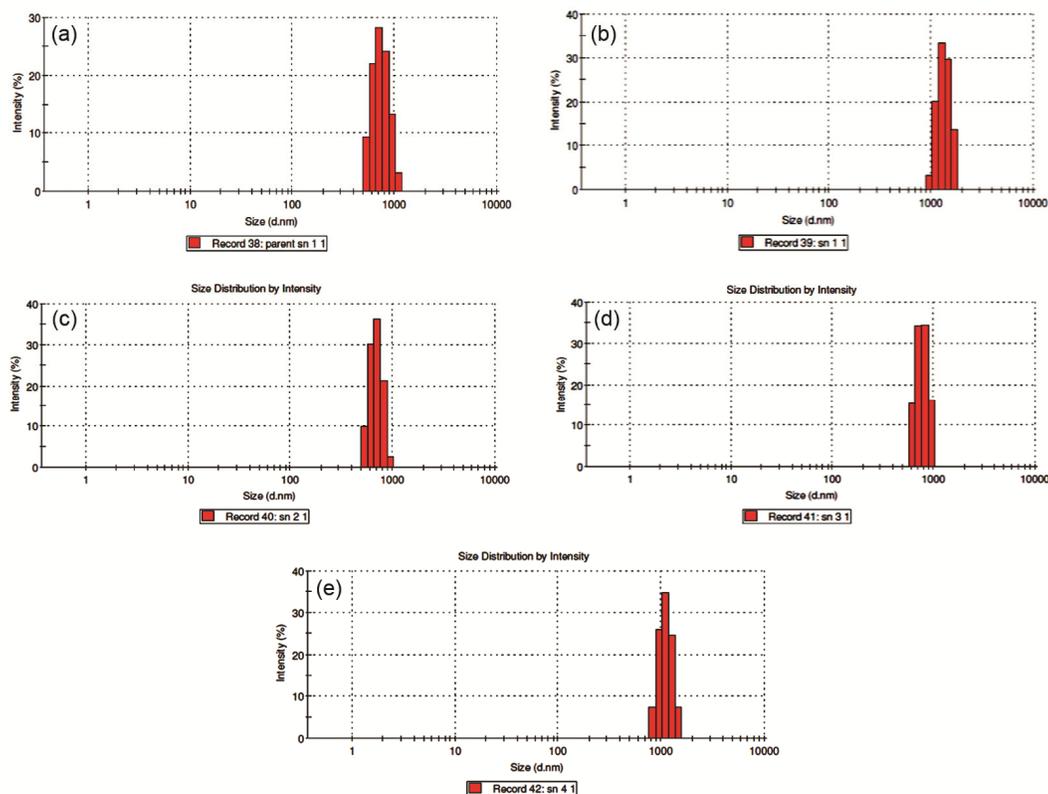
Fig. 4 — Particle size distribution curves obtained on Mn doped SnO_2 nanoparticles ((a) SnO_2; (b) $Sn_{0.95}Mn_{0.05}O_{2-\delta}$; (c) $Sn_{0.90}Mn_{0.10}O_{2-\delta}$; (d) $Sn_{0.85}Mn_{0.15}O_{2-\delta}$; (e) $Sn_{0.80}Mn_{0.20}O_{2-\delta}$.

Table 3 — Particle size data obtained on Mn doped SnO_2 nanoparticles

Sample	Average particle size (nm)
SnO_2	704.2
$Sn_{0.95}Mn_{0.05}O_{2-\delta}$	1258
$Sn_{0.90}Mn_{0.10}O_{2-\delta}$	859.4
$Sn_{0.85}Mn_{0.15}O_{2-\delta}$	956.8
$Sn_{0.80}Mn_{0.20}O_{2-\delta}$	1037

sized grains (> 500 nm) are also seen in some places. By doing the heat treatment process, the formation of micron sized grains in the ceramic structures can be controlled to a greater extent[32].

3.4 Absorbance Studies

The UV – Visible absorbance spectra obtained on Mn doped SnO_2 nanoparticles are indicated in Fig 6. The absorption wavelength of 283 nm was obtained for manganese doped tin oxide nanoparticles. Energy band gap values for all the samples were calculated by using Tauc relation (Equation 2).

$$(\alpha h\gamma)^n = A (h\gamma - E_g) \qquad ...(2)$$
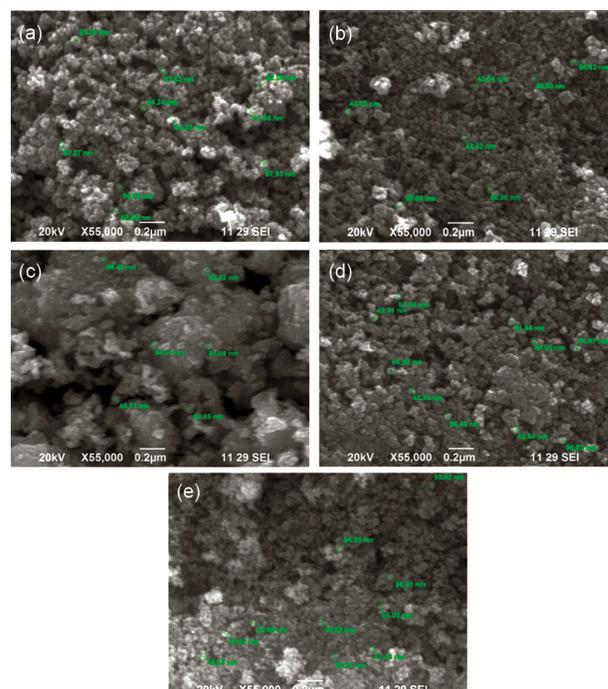
Fig. 5 — SEM photographs obtained on Mn doped SnO_2 nanoparticles (a) SnO_2; (b) $Sn_{0.95}Mn_{0.05}O_{2-\delta}$; (c) $Sn_{0.90}Mn_{0.10}O_{2-\delta}$; (d) $Sn_{0.85}Mn_{0.15}O_{2-\delta}$; (e) $Sn_{0.80}Mn_{0.20}O_{2-\delta}$.
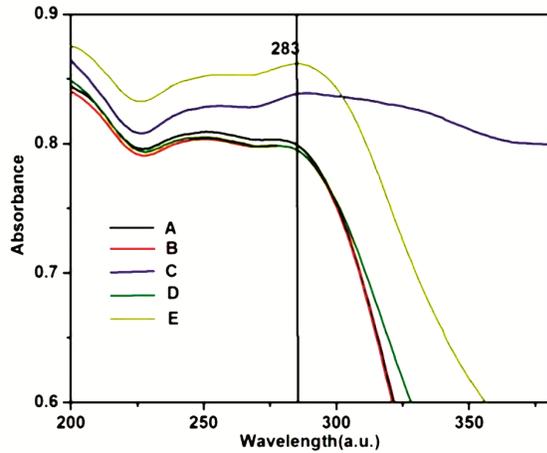
Fig. 6 — UV-Visible absorbance spectra obtained on Mn doped SnO$_2$ nanoparticles (a) SnO$_2$; (b) Sn$_{0.95}$Mn$_{0.05}$O$_{2-\delta}$; (c) Sn$_{0.90}$Mn$_{0.10}$O$_{2-\delta}$; (d) Sn$_{0.85}$Mn$_{0.15}$O$_{2-\delta}$; (e) Sn$_{0.80}$Mn$_{0.20}$O$_{2-\delta}$.
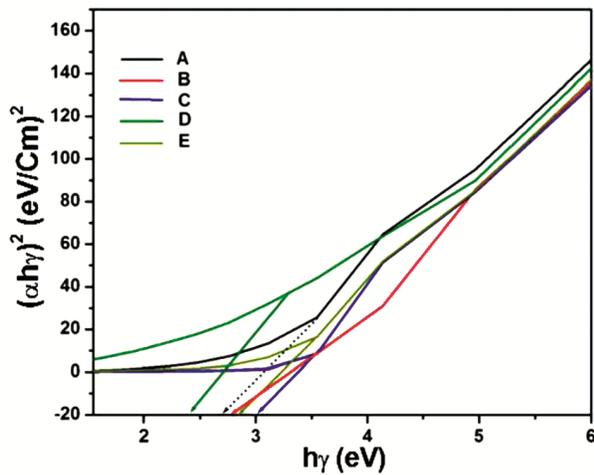
Fig. 7 — Band gap curves obtained on Mn doped SnO$_2$ nanoparticles (a) SnO$_2$; (b) Sn$_{0.95}$Mn$_{0.05}$O$_{2-\delta}$; (c) Sn$_{0.90}$Mn$_{0.10}$O$_{2-\delta}$; (d) Sn$_{0.85}$Mn$_{0.15}$O$_{2-\delta}$; (e) Sn$_{0.80}$Mn$_{0.20}$O$_{2-\delta}$.

Where 'α' is the absorption co-efficient, 'hγ' is the photo energy, 'E_g' is the optical band gap, 'A' is a constant relative to the material and 'n' is either 2 for direct transition, or ½ for an indirect transition. The optical band gap value for the direct transition for all the samples was obtained from Fig. 7. The calculated band gap values for the manganese doped tin oxide nanoparticles were found to be 2.6, 2.7, 3.0, 2.4 and 2.9 eV for the samples such as SnO$_2$, Sn$_{0.95}$Mn$_{0.05}$O$_{2-\delta}$, Sn$_{0.90}$Mn$_{0.10}$O$_{2-\delta}$, Sn$_{0.85}$Mn$_{0.15}$O$_{2-\delta}$ and Sn$_{0.80}$Mn$_{0.20}$O$_{2-\delta}$ respectively. The band gap values calculated for the manganese doped tin oxide nanoparticles were in agreement with the reported data. Sarangi *et al.*[33] have reported the band gap value for Pb doped SnO$_2$ as 2.87 eV - 3.64 eV.
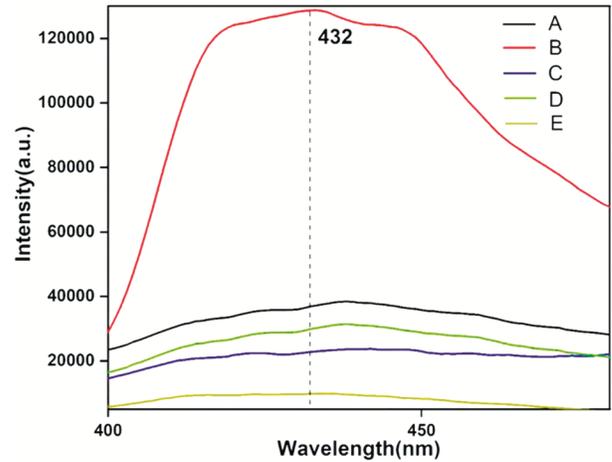
Fig. 8 — PL spectra obtained on Mn doped SnO$_2$ nanoparticles (a) SnO$_2$; (b) Sn$_{0.95}$Mn$_{0.05}$O$_{2-\delta}$; (c) Sn$_{0.90}$Mn$_{0.10}$O$_{2-\delta}$; (d) Sn$_{0.85}$Mn$_{0.15}$O$_{2-\delta}$; (e) Sn$_{0.80}$Mn$_{0.20}$O$_{2-\delta}$.

Photoluminescence studies

From the UV results, the excitation wavelength was fixed at 283 nm. Then, photoluminescence spectra were taken for Mn doped SnO$_2$ nanoparticles (Fig. 8). From the figure, we could identify strong and broad peaks for tin oxide and Mn doped tin oxide nanoparticles at around 450 nm which reflected the purity and crystallinity of the materials. From the Fig. 8, it is clear that strong peaks appeared at around 432 nm may due to the blue emission of the visible region[34].

3.5 Photocatalytic Studies

The photocatalytic degradation of the pollutant, methylene blue dye, was carried out in a photoreactor along with Sn$_{1-x}$Mn$_x$O$_{2-\delta}$ (where x = 0, 0.05, 0.10, 0.15 and 0.20) nanophotocatalysts under UV light, visible light and sunlight respectively at different time intervals, viz., 0, 30, 60, 90 and 120 minutes. For the analysis of UV light absorbance of the characteristic peak of methylene blue dye, the wavelength at 665 nm was chosen as the reference peak. The percentage of degradation was calculated from following formula (Equation 3).

The percentage of degradation = $((C_0 - C_t) / C_0) \times 100$
$$\ldots(3)$$

Where, C_0 is the initial absorbance of the dye solution and C_t is the absorbance at time interval respectively. The photodegradation curves obtained for methylene blue dye under the irradiation of UV, visible and sunlight in presence and absence
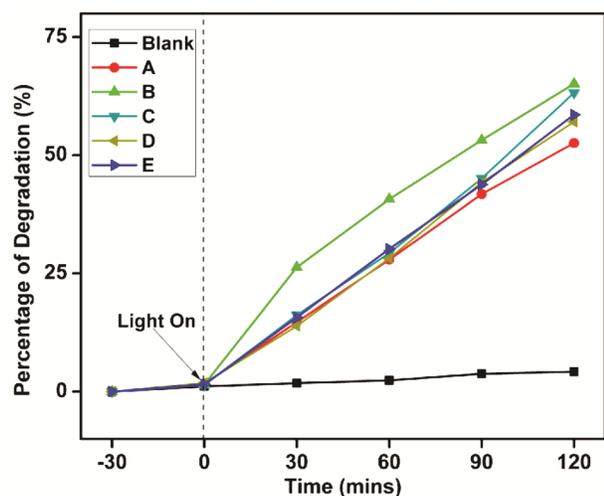
Fig. 9 — The photodegradation curves obtained for methylene blue under irradiation of UV light in presence and absence of Mn doped SnO_2 nanoparticles with respect to different to time intervals (a) SnO_2; (b) $Sn_{0.95}Mn_{0.05}O_{2-\delta}$; (c) $Sn_{0.90}Mn_{0.10}O_{2-\delta}$; (d) $Sn_{0.85}Mn_{0.15}O_{2-\delta}$; (e) $Sn_{0.80}Mn_{0.20}O_{2-\delta}$; Blank (absence of nanophotocatalyst).

Fig. 11 — The photodegradation curves obtained for methylene blue under irradiation of sun light in presence and absence of Mn doped SnO_2 nanoparticles with respect to different to time intervals (a) SnO_2; (b) $Sn_{0.95}Mn_{0.05}O_{2-\delta}$; (c) $Sn_{0.90}Mn_{0.10}O_{2-\delta}$; (d) $Sn_{0.85}Mn_{0.15}O_{2-\delta}$; (e) $Sn_{0.80}Mn_{0.20}O_{2-\delta}$; Blank (absence of nanophotocatalyst).

Fig. 10 — The photodegradation curves obtained for methylene blue unfder irradiation of visible light in presence and absence of Mn doped SnO_2 nanoparticles with respect to different to time intervals (a) SnO_2; (b) $Sn_{0.95}Mn_{0.05}O_{2-\delta}$; (c) $Sn_{0.90}Mn_{0.10}O_{2-\delta}$; (d) $Sn_{0.85}Mn_{0.15}O_{2-\delta}$; (e) $Sn_{0.80}Mn_{0.20}O_{2-\delta}$; Blank (absence of nanophotocatalyst).

of different compositions of Mn doped SnO_2 nanoparticles with respect to different time intervals are presented in Figs. 9, 10 and 11 respectively.

From the curves, it is clear that the photodegration is minimal for blank even after 120 minutes. Also, it is inferred that the photodegradation percentage could increase with respect to time. Under UV and visible light, sample b ($Sn_{0.95}Mn_{0.05}O_{2-\delta}$) showed better degradation percentage, viz., 65.1% and 84.8%

respectively after 120 minutes of exposure. Under sunlight, sample c ($Sn_{0.90}Mn_{0.10}O_{2-\delta}$) showed better result (45.8%) after 120 minutes of irradiation. From the results, it was confirmed that Mn doped SnO_2 nanoparticles can be the better photocatalysts in degrading organic dyes present in polluted water. As per the literature, Mn doped SnO_2 increased the photocatalytic efficiency by enhancing the charge separation and extended photo responding range. Further, uniform particle characteristics of the prepared materials may also one of the reasons for transferring both electrons and holes formed inside the crystal lattice uniformly which in turn enhanced the degradation of methylene blue dye solution[35].

4 Conclusions

Soft chemical synthesis can be effectively used to synthesize Mn doped SnO_2 ($Sn_{1-x}Mn_xO_{2-\delta}$; where x=0, 0.05, 0.10, 0.15 and 0.20) nanoparticles. The prepared ceramic particles were characterized by XRD, FTIR, particle size analysis, SEM, UV and PL studies. As per XRD, the particles are perfectly indexed to tetragonal geometry. Peaks appeared at 600 cm⁻¹ in all the samples may be relevant to SnO_2 frame work. The particles were present in between 50 to 100 nm and the presence of bulky particles may be to agglomeration effect. The band gap values for the samples were found in between 2.4 to 3.0 eV. The photoluminescence spectra of the samples exhibited a

strong peak at 432 nm. Among the samples studied, Sn$_{0.95}$Mn$_{0.05}$O$_{2-\delta}$ exhibited better photodegradation percentage (84.8%) in removing methylene blue dye under visible light after exposure for 120 minutes. Mn doped SnO$_2$ nanophotocatalyst can be a better choice in degrading the organic dyes present in polluted water.

Acknowledgement

References

1 Khan I, Saeed K & Khan I, *Arab J Chem,* 12 (2019) 908.
2 Baig N, Kammakakam I & Falath W, *Mater Adv*, 2 (2021)1821.
3 Guo D, Xie G & Luo J, *J Phys D Appl Phys*, 47 (2014) 013001.
4 Kujawa J & Kujawski W, *ACS Appl Mater Interfaces*, 8 (2016) 7509.
5 Gebreslassie Y T & Gebretnsae H G, *Nanoscale Res Lett*, 16 (2021) 97.
6 Bala Subbaiah G, Venkata Ratnam K, Janardhan S, Shiprath K, Manjunatha H, Ramesha M, Krishna P N V, Ramesh S & Anil B T, *Front Mater*, 8 (2021) 682025.
7 Umashanker L, Bharathesh T P, Roopashree C & Saravanan R, *IOP Conf Ser Mater Sci Eng*, 1189 (2021) 012015.
8 Ficai D, Oprea O, Ficai A & Holban AM, *Curr Proteomics*, 11 (2014) 139.
9 García M C, Torres J, Córdoba A V D, Longhi M & Uberman P M, *Metal Oxides for Biomedical and Biosensor Applications*, (2022) 35.
10 Cartwright A, Jackson K, Morgan C, Anderson A & Britt DW, *Agronomy*, 10 (2020) 1018.
11 Lu H, Wang J, Stoller M, Wang T, Bao Y & Hao H, *Adv Mater Sci Eng*, (2016) 4964828.
12 Chavali M S & Nikolva M P, *SN Appl Sci*, 1 (2019) 607.
13 Honarmand M, Golmohammadi M & Bakhtiari J H, *Environ Sci Pollu Res*, 28 (2021) 7123.
14 Ayeshamariam A, Vidhya VS, Sivaranjani S, Bououdina M, Perumal Samy R & Jayachandran M, *J Nanoelectron Optoelectron*, 8 (2013)1.
15 Karmaoui M, Jorge A B, McMillan P F, Aliev A E, Pullar R C, Labrincha J A & Tobaldi D M, *ACS Omega*, 3 (2018) 13227.
16 Krishnakumar T, Jayaprakash R, Singh V N, Mehta B R & Phani A R, *J Nano Res*, 4 (2009) 91.
17 Tazikeh S, Akbari A, Talebi A & Talebi E, *Mater Sci – Pol*, 32 (2014) 98.
18 Bhattacharjee A, Ahmaruzzaman Md & Sinha T, *RSC Adv*, 14 (2014) 51418.
19 Akhir M A M, Mohamed K, Lee H L & Rezan S A, *Procedia Chem*, 19 (2016) 993.
20 Durga P P, Reddy S P, Deepthi A, Prashanthi J & Rao GN, *Int J Nanotechnol Appl*, 11 (2017) 265.
21 Wan W, Li Y, Ren X, Zhao Y, Gao F & Zhao H, *Nanomater. (Basel)*, 8 (2018) 112.
22 Liu Y, Jiao Y, Qu F, Gong L & Wu X, *J Nanomater*, (2013) 610964.
23 Inderan V, Lim S Y, Ong T S, Bastien S, Braidy N & Lee H L, *Superlattices Microstruct*, 88 (2015) 396.
24 Shehzad K, Shah NA, Amin M, Abbas M & Syed WA, *Int J Distrib Sens Netw*, 14 (2018) 1.
25 Meng X, Zhou M, Li X, Yao J, Liu F, He H, Xiao P & Zhang Y, *Electrochim Acta,* 109 (2013) 20.
26 Mali S S, Patil J V, Kim H & Hong C K, *Nanoscale*, 10 (2018) 8275.
27 Sharma D, Tripathi S, Panwar R S, Dhillon G, Bhatia A K, Vashisht D, Mehta S K & Kumar N, *Vacuum*, 184 (2021) 109925.
28 Bae J Y, Park J, Kim H Y, Kim H S & Park J S, *ACS Appl Mater Interfaces*, 7 (2015) 12074.
29 Aziz M, Abbas S S & Baharom W R W, *Mater Lett*, 91 (2013) 31.
30 Farrukh M A, Heng B T & Adnan R, *Turk J Chem*, 34 (2020) 537.
31 Mourdikoudis S, Pallares R M & Thanh N T K, *Nanoscale*, 10 (2018) 12871.
32 Belyakov AV, *Refract Ind Ceram,* 60 (2020) 574.
33 Sarangi N, Pradhan G K & Samal D, *J Alloys Compd*, 762 (2018)16.
34 Wang Y, Yu Y, Zou Y, Zhang L, Hu L & Chen D, *RSC Adv*, 8 (2018) 4921.
35 Prakash K, Senthil Kumar P, Pandiaraj S, Saravanakumar K & Karuthapandian S, *J Exp Nanosci*, 11 (2016) 1138.